Pure multistep oriented attachment growth kinetics of surfactant-free SnO2 nanocrystals

ARTICLE *in* PHYSICAL CHEMISTRY CHEMICAL PHYSICS · OCTOBER 2009

Impact Factor: 4.49 · DOI: 10.1039/b907967j · Source: PubMed

5 AUTHORS, INCLUDING:

Zanyong Zhuang
Chinese Academy of Sciences
15 PUBLICATIONS **132** CITATIONS
SEE PROFILE

Jing Zhang
Fourth Military Medical University
698 PUBLICATIONS **10,032** CITATIONS
SEE PROFILE

Zhang Lin
Chinese Academy of Sciences
102 PUBLICATIONS **1,626** CITATIONS
SEE PROFILE

Pure multistep oriented attachment growth kinetics of surfactant-free SnO_2 nanocrystals

Zanyong Zhuang, Jing Zhang, Feng Huang, Yonghao Wang and Zhang Lin*

Received 21st April 2009, Accepted 15th June 2009
First published as an Advance Article on the web 27th July 2009
DOI: 10.1039/b907967j

In this work, crystal growth kinetics of surfactant-free nanocrystalline SnO_2 in distilled water at 175–250 °C were investigated. The growth rate followed the type of asymptotic curve in hundreds of hours, which could be fitted by the multistep oriented attachment (OA) kinetic model. High-resolution transmission electron microscope (HRTEM) data also indicated crystal growth occurring *via* the multistep OA mechanism. During the growth of SnO_2, the concentration of Sn ions in the aqueous solution was examined. It reveals that the unsaturated situation of SnO_2 results in crystal growth *via* the pure OA mechanism. A growth model of self-integration of conjugated nanocrystals was discussed for understanding the OA behavior.

1. Introduction

Nanoscale materials, such as ZnO, ZnS, SnO_2, have been investigated widely for their unique size-dependent properties of optics, electricity, and magnetism.[1,2] To tailor the properties of nanoparticles for specific applications, it is essential to develop a fundamental understanding of the nucleation and growth process.[3–5] Generally in the solution-based synthesis, nanocrystal growth processes are mainly controlled by two competitive mechanisms, Ostwald Ripening (OR) and Oriented Attachment (OA). In principle, the OR involves the growth of larger crystals at the expense of smaller ones by the way of ion diffusion,[6–8] while the OA occurs when nanoparticles with the common crystallographic orientation collide and directly combine together to form a larger one.[9–12]

Crystal growth *via* the OA or OR often shows unique characteristics, respectively. For example, the OR mechanism normally produces nanoparticles with regular shapes and few defects, while the OA usually results in nanoparticles with irregular morphologies and typical defects of twins, stacking faults, and misorientations.[9,13] Additionally, in respect of size evolution, the OR growth follows a parabola trend, which can be fitted by the classical LSW kinetic model.[6–8] Distinctively, the OA growth reveals an asymptotic curve, well described and fitted by the "molecular-like" OA kinetic model.[13]

Therefore, since the OA and OR often take place simultaneously during the hydrothermal growth of nanoparticles,[13–15] it brings difficulties to the in-depth studies on the nanocrystal growth kinetics. Promisingly, it has been found that introducing the strong surface adsorption is an effective approach to control over the coarsening of ZnS and PbS nanoparticles. So at the earlier stage of the growth, the OR is hindered and it is only controlled by the solo OA mechanism.[16–18] Furthermore, it is also suggested that the OR could be thermodynamically prohibited under an unsaturated solution (nanoparticles dissolving but not precipitating). Nevertheless, although work stated above has been done, currently kinetic studies on the OA phenomena are still so scarce that we have not enough data to grasp how and why the OA behavior could happen, since kinetic examples of nanoparticles grown *via* pure OA are difficult to be found.

Interestingly, Leite *et al.* reported that even without any surfactant, the growth of nanoparticles SnO_2 in water at 100–200 °C (within 200 h) was mainly controlled by the OA mechanism.[19–21] It was suggested that the OR was unfavorable in this process due to the small solubility of SnO_2 nanoparticles in water. Therefore, since previously we have noticed that, the occurrence of pure OA by inhibiting the OR is tightly related to the solubility, dissolving rate, surface state of nanoparticles, and the unsaturated state of solution, here we select nanocrystal SnO_2 to further investigate its growth kinetics, not only because of its size-dependent properties widely used for optoelectronic devices, gas sensors and other interesting areas,[22,23] but also its extremely small solubility potentially achieving the pure OA-based growth in a longer time scale.

Thus in this work, crystal growth of surfactant-free nanocrystalline SnO_2 in distilled water at 175–250 °C was investigated, where the hydrothermal time was prolonged to hundreds hours. Meanwhile, the variation of Sn ion concentration in the aqueous solution was also monitored, aiming to explore the relationship between nanocrystal dissolution and the OA-based growth. Significantly, different from previous work,[19,20] our data showed that not only the OA between two primary nanoparticles, but also the attachment between multilevel ones existed in the growth of SnO_2 nanoparticles. So the SnO_2–water system was reported here as new kinetic example for the studies on the multistep OA mechanism, which can be well explained by the developed multistep OA kinetic model. Additionally, the size distribution evolution of nanoparticles SnO_2 during OA growth was also investigated, and a growth model of self-integration of conjugated nanocrystals was proposed to understand the OA behavior.

State Key Lab of Structural Chemistry Fujian Institute of Research on the Structure of Matter, Chinese Academy of Sciences, Fuzhou, Fujian 350002, People Republic of China. E-mail: zlin@fjirsm.ac.cn; Tel: +86 591 83705474

2. Experimental

The primary SnO_2 nanoparticles without any surface adsorption were synthesized in aqueous solution at room temperature. $SnCl_4{\cdot}5H_2O$ was dissolved in distilled water, and ammonium hydroxide was dropped into the solution under stirring. When the PH was $\sim$5, the mixture was centrifuged and washed with distilled water till Cl^- beyond the detection by 0.1 M $AgNO_3$ solution. Finally the product was dried and ground into powder for the following experiments.

As-synthesized nanoparticles SnO_2 (0.1 g) and 10 mL of distilled water were mixed and scaled into a Teflon-lined stainless steel autoclave with 23 mL capacity. The autoclaves were heated at 175, 210, 230, and 250 °C, respectively. For time series experiment, autoclave containers were taken out at the appropriate time interval. The hydrothermal bomb was quenched to room temperature with ice water only in 1–2 min to guarantee the re-dissolve/precipitation process as less as possible. This is also the classic method for obtaining the concentration situation in hydrothermal bomb. After fast cooling, we found the supernatant was clear. During experiments, if there was some re-precipitation process happen, such as in slightly dissolved ZnS or SnO_2 systems, we found normally it took tens of minutes to observe the cloudy precipitates. Finally, the precipitates were collected and washed with anhydrous ethanol until the PH was $\sim$7.

To check whether or not SnO_2 nanoparticles in hydrothermal solution reached the dissolve/precipitation equilibrium, procedures were done as follows. After hydrothermally treated for hours, the autoclave containers were taken out and quenched to room temperature. The clear supernatant was quickly extracted and further centrifuged at the speed of 8000 rpm for 1 minute. The whole process was done within 4–5 min. 2 mL of the supernatants were taken for the detection of Sn ion concentration by Inductively Coupled Plasma (ICP) (Ultima2). To affirm no SnO_2 nanoparticles included in the supernatant, we re-dissolved the as-precipitated-and-dried SnO_2 into 10 mL distilled water at room temperature. After vigorously agitating for 5 minutes, the solution became cloudy; then, the same process of centrifuge as above was done. We repeated the centrifuging treatment for 4 times. It showed an average value of 0.9 mg/L of Sn ions in the supernatant. Therefore, compared to the concentration value in Fig. 6 (from about 4 to 17 mg/L), it was proved that little nanoparticles stayed in the supernatant after rapid centrifuge.

The crystal structures and the average sizes of samples were identified by a PANalytical X' Pert PRO diffractometer with Cu Kα radiation (40 kV, 40 mA) in the continuous scanning mode. The 2θ scanning range was from 15° to 75° in steps of 0.03° with a collection time of 35 s per step. Hence, the average crystallite size could be calculated from peak broadening by using the Scherrer equation.

Since the accuracy of particle sizes extracted from XRD patterns are closely related to the background and peak profile analysis, so here we also specify the procedure of analysis on these two aspects. Firstly, for XRD pattern of powder, once the background contains no structural factor, it is mainly caused by the fluorescence effect. As we all know, for bulk material it can be easily deducted. While once the size of particle reduces to small nanoscale, it is difficult to distinguish the true background from the broadening peak. Normally at this time, the background deduction in small nanoparticles case could be carried on, according to the background obtained in bulk materials, since backgrounds in nanoscale and bulk materials generated by the fluorescence effect can be approximately equivalent. After the background deduction, as shown in eqn (1), here we use Pearson VII function to describe peak shapes of XRD patterns observed in our experiment.

$$f(x) = a\left[1 + \frac{(x-d)^2}{b^2}\right]^{-m} \quad (1)$$

where (d,a) are the coordinates of the peak maximum, exponent m is a shape factor that determines the rate at which the tails fall, and b is proportional to the full width at half-maximum (FWHM). Special cases of this function are that it becomes a Cauchy as $m = 1$, a modified Lorentzian as $m = 2$, and approaches a Gaussian as $m \to \infty$ (*e.g.* $m > 10$). So to obtain the error in peak broadening parameter (FWHM), we set the shape parameter m at 1 and 10. Thus different functions are gained at two extremes, and used to analyse the peak profile of XRD pattern, respectively. While in the two extreme cases, the extracted value of peak wide parameter can be relatively accurate, only the peak profile fitting is not so ideal. Based on this, the domain that parameter FWHM varies can be obtained, and the error is extracted.

In addition, High-resolution transmission electron microscopy (JEOL JEM2010 HRTEM at 200 kV) was also used to confirm the sizes, sizes distributions, and morphologies of nanoparticles.

3. Results

Fig. 1 shows the typical XRD pattern and HRTEM image of as-synthesized SnO_2 nanoparticles. XRD data reveal that the nanoparticles are in the tetragonal phase, with a calculated average size of $\sim$1.9 nm in [110], [101], and [211] directions, which is also confirmed by HRTEM observations.

SnO_2 nanoparticles after hydrothermally treated in distilled water were characterized with the same methods as above. Fig. 2a–d show the increase of average particle sizes *versus* time at 175, 210, 230, and 250 °C. It reveals that, the growth of SnO_2 particles at different temperatures share the same rule, following an asymptotic cure, while the experimental data can not be fitted to LSW model, with $n = 6$ bearing no physical meaning. Therefore, the growth of SnO_2 nanoparticles is not

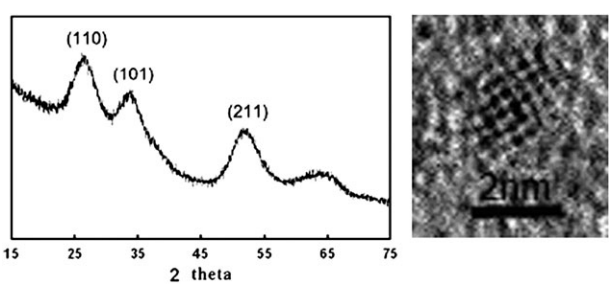

Fig. 1 XRD pattern (left) and HRTEM image (right) of the as-synthesized SnO_2 nanoparticles.

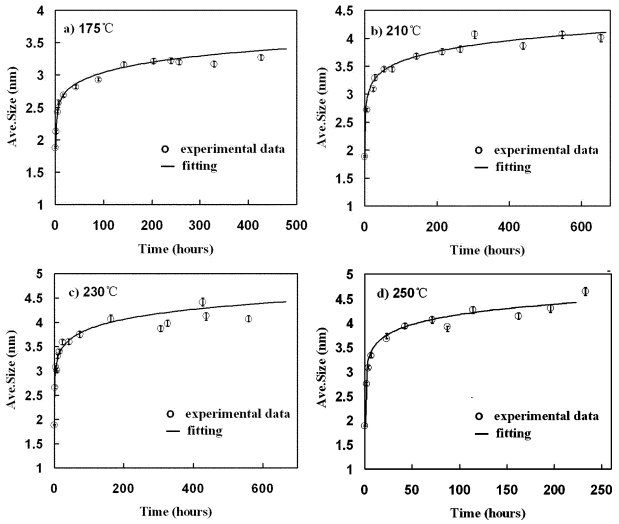

Fig. 2 Experimental data and fitting results showing the mean size as a function of time at each temperature.

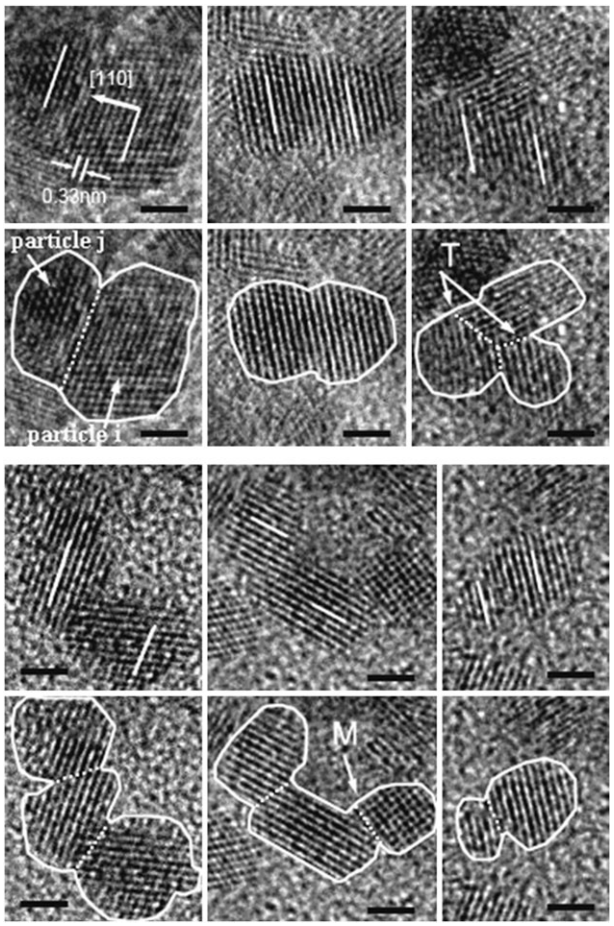

Fig. 3 Typical HRTEM images of samples hydrothermally treated at 250 °C for 4 h in distilled water. Small particles as "building block" attach with each other *via* a common crystallographic orientation to form a larger one. The white parallel lines highlight the orientation between two parallel (110) facets. Schematic outlines of each image illustrate the attachment scheme of OA and the defects forming during the OA growth, such as twins (T) and misorientations (M). Scale bars: 2 nm.

controlled by the OR. Additionally, the maximum size of SnO_2 particles grown at each temperature approaches 3.2, 4.0, 4.1, and 4.2 nm, respectively, all of which are about 5–12 times of the primary ones in volume.

To further investigate the growth mechanism of nanoparticles SnO_2, HRTEM observations were collected. Fig. 3 shows the typical HRTEM images of SnO_2 nanoparticles by hydrothermal treatment in distilled water at 250 °C for 4 h. All the crystals display the characteristics of OA mechanism. Small particles as "building block" attach with each other *via* a common crystallographic orientation (*i.e.* along the [110] direction shown in Fig. 3). Therefore, it indicates that the OA mechanism exists widely in the growth of nanoparticles SnO_2. However, different from previous $A_1 + A_1$ growth kinetics for SnO_2,[19,20] it is obviously found in our experiment that not only OA between primary SnO_2 particles but also attachment between two multilevel ones can occur. For example, the multilevel particles *i* and *j* in Fig. 3 combined into a new and single crystal *via* the OA mechanism, while the two nanoparticles themselves might be the products of a multi-OA reaction, due to their larger size than that of primary particles ($\sim$1.9 nm). Similar phenomenon can be observed commonly in the growth of nanoparticles SnO_2. Combined with the statements above, the growth of nanoparticles SnO_2 is controlled by a multistep OA mechanism, which is consistent with the result shown in Fig. 2 that the maximal nanoparticles SnO_2 are about 5–12 times of the primary ones in volume.

4. The fitting by the multistep OA kinetic model

The results shown as above reveal that the growth in SnO_2 system is controlled by the multistep OA mechanism. So here we use the built multistep OA kinetic model to fit the growth curves of SnO_2 nanoparticles.[16]

It is suggested that under hydrothermal treatment, the OA of nanoparticles is similar to the reaction between molecules,[9,24] and then can be described as follows:

$$A_i + A_j \xrightarrow{K_{ij}} A_k (i,j,k = 1,2,...) \qquad (2)$$

A_k is the particle which contains k primary particles, and $k = i + j$. K_{ij} is the rate constant for the reaction between the particles. So the time evolution of the concentration of A_k describes the sum of the formation and loss of the particles. The hypotheses in the growth are (a) the reaction is an irreversible, random, and binary one between A_i and A_j, and (b) spatial fluctuations in particle density and particle shape are neglected. Therefore, the rate matrix K_{ij} is given as:[16]

$$K_{ij} = 4\pi R_1 D_1 (i^{1/3} + j^{1/3})(i^{\alpha} + j^{\alpha}) \qquad (3)$$

where R_1 and D_1 are the radius (0.95 nm for SnO_2) and diffusion coefficient of primary particle, and α is a constant. According to the definition of the volume-weighted average particle size,[25] the average size at this certain moment, d_{eq}, can be obtained by:

$$d_{eq} = \sum N_k d_k^4 / \sum N_k d_k^3 \qquad (4)$$

Table 1 Estimated values by fitting the experimental data at each temperature

T (°C)	R_1	K_1 ($=D_1N_1(0)$)	α
175	0.9	3.0×10^3	−4
210	0.9	3.0×10^4	−4
230	0.9	8.6×10^4	−4
250	0.9	2.5×10^5	−4

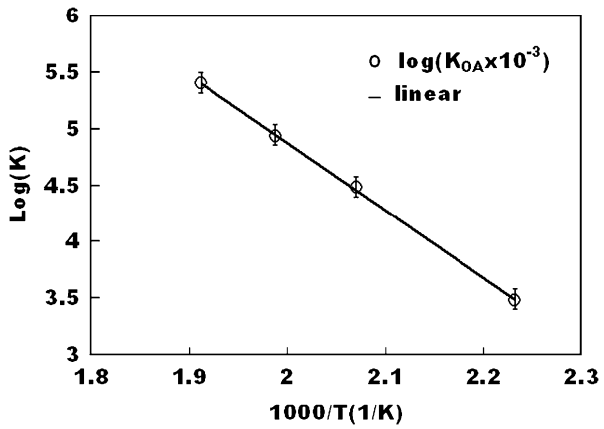

Fig. 4 Arrhenius plot of the fitting kinetic constant for OA mechanism.

where d_k is the size of particle containing k primary particles. Thus, the increasing particle size with time revolution will be calculated.

The fitting growth curves of SnO_2 nanoparticles are shown in Fig. 2, and the parameters of fitting result are shown in Table 1. Results revealed that the growth of nanoparticles SnO_2 is mainly controlled by a multistep OA mechanism, which can last for a relative long time without any surface adsorption. It also shows that the SnO_2-water system is the new example for the built multistep OA mechanism, which can be well explained by the multistep OA kinetic model ($A_i + A_j$).

The apparent activation energy of OA in SnO_2-water system can also be obtained as follow. The kinetic constants vary with temperature and can be described by the Arrhenius equation:

$$\log K = -\frac{Ea}{RT} + A_0 \qquad (5)$$

Here, Ea is the apparent activation energy, A_0 is the pre-exponential factor, R is the universal gas constant, and T is the absolute temperature. Fig. 4 shows the Arrhenius plot of kinetic constants K. Here we take $K = N_{1(0)}D_1$ as the apparent kinetic constant of OA, for ($N_{1(0)}D_1$) is an integral factor and α is a constant independent of temperature. From the Arrhenius plot of various kinetic constant, we obtained the apparent activation energy of OA, Ea (K_{OA}) = 49.7 ± 4.8 KJ/mol.

5. Discussion

5.1 The size distribution evolution of SnO_2 nanoparticles during the OA growth

Due to the size-dependent properties, in this work, the size distribution evolution of SnO_2 nanoparticles during the OA growth was also investigated, based on TEM statistics on three SnO_2 samples.

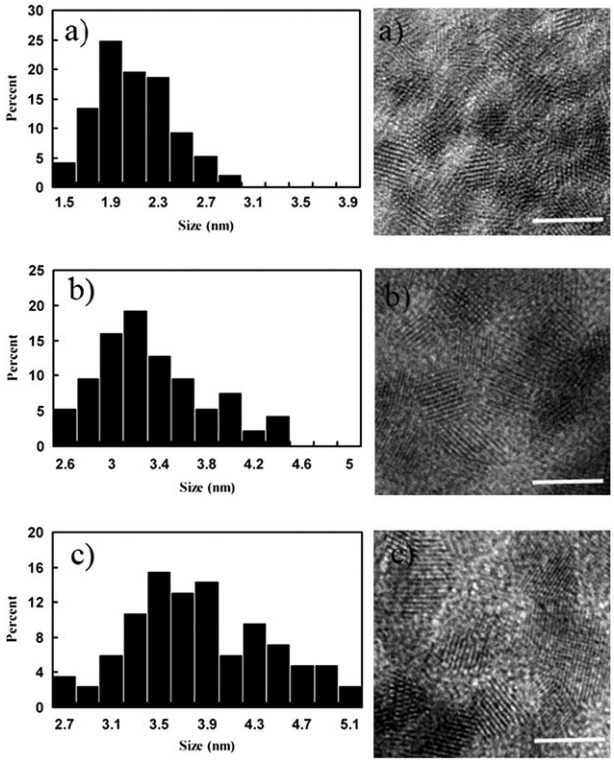

Fig. 5 Size distributions and HRTEM images of samples, (a) primary, (b) after treated at 250 °C for 4 h. (c) after treated at 250 °C for 42 h. Scale bars: 5 nm.

As shown in Fig. 5, firstly, it clearly reveals that, before treated the primary SnO_2 sample has possessed a size distribution in the range from 1.5 to 2.9 nm, with highest probability at 1.9 nm. This result is basically consistent with the truth that the primary particle size calculated from XRD is about 1.9 nm. Further it also demonstrates that, as OA growth proceeding, the distribution seems gradually broaden. While after hydrothermally treated for 42 hours, it presents a size range from 2.7 to 5.1 nm, which is much broader than the primary one.

Interestingly, the broadening size distribution of SnO_2 nanoparticles in OA growth stated above, is basically consistent with the observation found in ZnS–NaOH system.[16] While previously it has revealed that, even if the primary ZnS sample was set at zero-distribution (such as 2.4 nm), by calculated from the built multistep OA kinetic model, the OA growth itself could bring a size distribution. Since in reality, the primary one has already possessed a size distribution, thus after OA growth, the actual size distribution of ZnS nanoparticles count from TEM images would be broader than the calculated results.

Additionally, based on TEM statistics, the average sizes of samples were also extracted, and used to corroborate the calculated values from XRD, since the extraction of grain sizes from XRD pattern of small nanoparticles might introduce high errors.[26] As shown in Table 2, the average sizes of three samples were both analysed by XRD and TEM. It revealed the

Table 2 Comparison of particles sizes by XRD and TEM analysis. (s = standard deviation, and σ = standard error)

Sample	XRD (nm)	TEM
Primary	1.9 ± 0.1	Highest probability at 1.9 nm, with s = 0.32 nm, σ = 0.03 nm
Treated at 250 °C for 4 h	3.1 ± 0.3	Highest probability at 3.2 nm, with s = 0.64 nm, σ = 0.06 nm
Treated at 250 °C for 42 h	3.9 ± 0.5	Highest probability at 3.5 nm, with s = 0.70 nm, σ = 0.07 nm

calculated results from XRD are basically consistent with TEM statistics. Although there is a small deviation, it is reasonable since the existence of lattice distortion of small nanoparticles.

5.2 The relationship between the unsaturated situation of nanoparticles and pure OA kinetics

As reported in the coarsening of PbS and ZnS,[16–18] both the surface adsorption and solution situation can play critical roles in generating a pure OA-based growth.

(1) For dodecanethiol-capped nanocrystals PbS grown in water,[18] the capping agents on nanoparticles surface hinder the OR growth, thus primary particles basically grow *via* the OA mechanism. However, as an organic ligand, thiol is an unstable surface adsorption agent under coarsening treatment, which can be destroyed and desorbed into water at hydrothermal condition. Especially for secondary particles and multilevel ones built by the OA of primary particles, the adsorbed species may be irreversibly removed from the interface during the coalescence. With the desorption of surface thiol agents, the dissolution/precipitation process of particles will not be hindered as before. The tendency for secondary and multilevel particles grown by OR mechanism becomes prominent. Thus it leads to the low possibility of OA between multilevel particles and a relative short OA dominant period.

(2) For nanocrystals ZnS coarsening in concentrated NaOH,[16,17] the surface adsorption of OH– is so strong that it prevents the achievement of saturation equilibrium of solution. Thus the OR growth of primary particles is prohibited thermodynamically, and OA mechanism controls the crystal growth. Moreover, as an inorganic agent, the surface adsorption of NaOH is relatively stable during coarsening, which provides strong surface adsorbent continuously. The newly formed coalescent multilevel nanoparticles are also immediately surrounded by the strong surface adsorbent. Thus the probability of OA between multilevel nanoparticles is also very high and the multistep OA growth process was observed at large size range.

Interestingly, the growth of SnO_2 in water and ZnS in concentrated NaOH,[16,17] share the same characteristics of a relative long-time multistep OA process. Differently there is no surfactant in SnO_2-water system. Hence, we propose that the pure OA-based growth in SnO_2 system might be also related to the coarsening solution.

To verify this, we checked the concentration of tin ions in solution as time increased at 250 °C. Results shown in Fig. 6

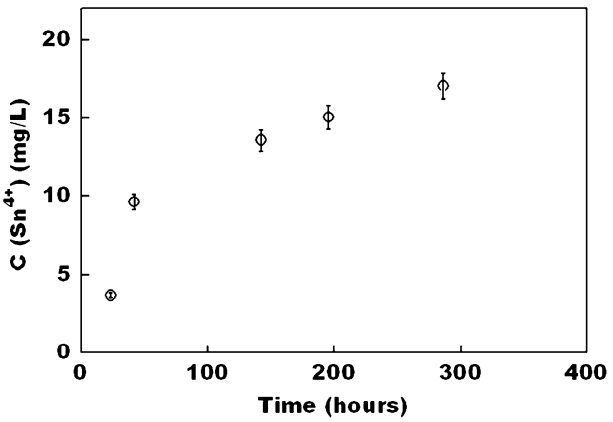

Fig. 6 ICP results showing the Sn ion concentration *vs.* time in water at 250 °C.

revealed that the solution was far from saturated through out the hydrothermal time. In principle, during hydrothermal growth of nanoparticles, an unsaturated condition of the solution can thermodynamically prohibit the OR process, because both the large and small particles will tend to dissolve in the unsaturated solution. On the other hand, when particles reduce to nanoscale size, OA can be dominant in the growth, due to the high surface energy and fast Brown motion of nanoparticles. Therefore, on the consideration of the unsaturated solution and the small sizes (several nanometres) of nanoparticles SnO_2, OR is prohibited thermodynamically and a relative long-time pure OA process might be obtained, which is beneficial to the OA between multilevel particles.

5.3 The model of self-integration during OA process

To the best of our knowledge, the OA mechanism usually generates anisotropic nanoparticles, such as chain-like TiO_2.[27] However, TEM data in our experiment revealed that, most of SnO_2 nanoparticles grown *via* a pure OA tended to be round, while only a few anisotropic particles (*i.e.* shown in Fig. 3) can be found. Similar phenomenon was also reported in the coarsening of ZnS.[16] One should keep in mind that the reasons we deduce the growth of SnO_2 nanoparticles *via* a pure OA, with neglectable OR, are based on the following facts. (1) The growth rate of SnO_2 followed the typical asymptotic curve of OA process in hundreds of hours. If SnO_2 grew *via* OR or OA + OR, it should follow the parabola-type growth curve.[13] (2) The data from the Sn ion concentration experiment clearly showed an unsaturated situation in the growth of SnO_2. Therefore, OR was basically prohibited, for both the large and small particles would tend to dissolve thermodynamically in a solution far from saturated. Additionally, our HRTEM images presented the direct proof of the OA-based growth.

Therefore, to explain the morphology of SnO_2 formed by the OA and get a deeper understanding of the OA behavior, a growth model of self-integration of conjugated nanocrystals during OA was proposed. As shown in Fig. 7, we suggest that the self-integration effect during the OA process might undergo state A, B and C. Generally, state A is formed *via* OA firstly. However, it is hardly observed by HRTEM observations in this and previous work. Thus we proposed

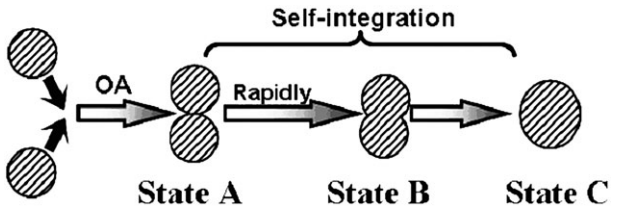

Fig. 7 Schematic illustrating the self-integration effect during OA process.

the self-integration from A to B is very rapid. According to Gibbs–Thompson equation,

$$\mu = \frac{2\gamma\Omega}{R} \qquad (6)$$

where μ is the chemical potential, γ is the surface free energy, Ω is volume per atom, and $1/R$ is the radius curvature. As the radius curvature at the joint of particles at the state A and B is negative, the chemical potential there should be minus. Thus, atoms sited on other place are thermodynamically favored to move to the joint. Thus self-integration from state B to state C is favored in energy. In another word, with time extending, the final shape of particles generated by OA tends to be regular as state C.

By comparing with the some examples reported (TiO_2, ZnS, SnO_2 and so on), it is found that the OA mechanism could generate particles with different morphologies. We think that it is the lattice energy and size of nanoparticle that determine the rate of self-integration from state B to C, ultimately resulting in particles with regular morphologies or not. On one hand, when the lattice energy of the nanoparticles is low enough (such as in ZnS, PbS system), nanoparticles will quickly self-integrate into regular shape and the typical OA feature can hardly be captured. On the contrary, in TiO_2 or FeOOH system with high lattice energy, typical OA feature and anisotropic shape can be easily observed. On the other hand, the speed of self-integration can also be influenced by the sizes of particles. Although SnO_2 has a high lattice energy similar to rutile, the shape of nanoparticles SnO_2 growing *via* OA tend to be regular. Compared to TiO_2 with size about tens of nanometres, the small size of nanoparticles SnO_2 ($\sim$2–5 nm) is beneficial to the self-integration. For the high surface energy and high surface-volume ratio make the nanoparticles SnO_2 at state B a high reactivity, which favors the self-integrate of nanoparticles to the state C.

6. Conclusions

Hydrothermal growth of nanoparticles SnO_2 *via* a relative long-time and pure multistep OA was investigated. It revealed that the growth rates followed the type of asymptotic curve, and could be well fitted by previous multistep OA kinetic model. During this process, the concentration of tin ions in the aqueous solution was also monitored. It disclosed that an unsaturated solution resulted in crystal growth *via* pure multistep OA mechanism. Additionally, size distributions of nanoparticles during OA growth were analyzed, and a growth model of self-integration of conjugated nanocrystals was proposed, to probe the understanding on the OA behavior.

Acknowledgements

We thank Bao Feng at Fujian Institute of Research on the Structure of Matter, Chinese Academy of Sciences, for helping with the TEM. Financial support for this study was provided by the Knowledge Innovation Project of The Chinese Academy of Sciences (KJCX1.YW.07), Outstanding Youth Fund (50625205), NNSF of China (20501020, 20501021, 20803082).

Notes and references

1 M. Law, H. Kind, B. Messer, F. Kim and P. Yang, *Angew. Chem.*, 2002, **144**, 2511.
2 C. Xu, J. Tamaki, N. Miura and N. Yamazoe, *Sens. Actuators, B*, 1991, **3**, 147.
3 F. Huang and J. F. Banfield, *J. Am. Chem. Soc.*, 2005, **127**, 4523.
4 I. Bilecka, P. Elser and M. Niederberger, *ACS Nano*, 2009, **3**, 467.
5 T. Hyeon, S. S. Lee, J. Park, Y. Chung and H. B. Na, *J. Am. Chem. Soc.*, 2001, **123**, 12798.
6 C. Z. Wagner, *Elektrochem.*, 1961, **65**, 581.
7 M. V. Speight, *Acta Metall.*, 1968, **16**, 133.
8 H. O. K. Kircher, *Metall. Trans.*, 1971, **2**, 2861.
9 R. L. Penn and J. F. Banfield, *Science*, 1998, **281**, 969.
10 R. L. Penn and J. F. Banfield, *Am. Mineral.*, 1998, **83**, 1077.
11 Z. L. Wang, *J. Phys. Chem. B*, 2000, **104**, 1153.
12 Z. Y. Tang, N. A. Kotov and M. Giersig, *Science*, 2002, **297**, 237.
13 F. Huang, H. Zhang and J. F. Banfield, *J. Phys. Chem. B*, 2003, **107**, 10470.
14 F. Huang, H. Zhang and J. F. Banfield, *Nano Lett.*, 2003, **3**, 373.
15 H. Zhang and J. F. Banfield, *Am. Mineral.*, 1999, **84**, 528.
16 J. Zhang, Z. Lin, Y. Lan, G. Ren, D. Chen, F. Huang and M. Hong, *J. Am. Chem. Soc.*, 2006, **128**, 12981.
17 Y. Wang, J. Zhang, Y. Yang, F. Huang, J. Zheng, D. Chen, F. Yan, Z. Lin and C. Wang, *J. Phys. Chem. B*, 2007, **111**, 5290.
18 J. Zhang, Y. Wang, J. Zheng, F. Huang, D. Chen, Y. Lan, G. Ren, Z. Lin and C. Wang, *J. Phys. Chem. B*, 2007, **111**, 1449.
19 C. Ribeiro, E. J. H. Lee, E. Longo and E. R. Leite, *ChemPhysChem*, 2005, **6**, 690.
20 E. J. H. Lee, C. Ribeiro, E. Longo and E. R. Leite, *Chem. Phys.*, 2006, **328**, 229.
21 E. R. Leite, T. R. Giraldi, F. M. Pontes, E. Longo, A. Beltran and J. Andres, *Appl. Phys. Lett.*, 2003, **83**, 1566.
22 J. Ba, D. F. Rohlfing, A. Feldhoff, T. Brezesinski, I. Djerdj, M. Wark and M. Niederberger, *Chem. Mater.*, 2006, **18**, 2848.
23 Y. D. Wang, I. Djerdj, M. Antonietti and B. Smarsly, *Small*, 2008, **4**, 1656.
24 J. F. Banfield, S. A. Welch, H. Zhang, T. T. Ebert and R. L. Penn, *Science*, 2000, **289**, 751.
25 E. Kaelble, *Handbook of X-Rays*, Mcgraw-Hill, New York, 1967, pp. 17–18.
26 F. Huang, B. Gilbert, H. Zhang and J. F. Banfield, *Phys. Rev. Lett.*, 2004, **92**, 155501.
27 R. L. Penn and J. F. Banfield, *Geochim. Cosmochim. Acta*, 1999, **63**, 1549.